Research Article
Vol. 25, No. 15 | 24 Jul 2017 | OPTICS EXPRESS 18131
Optics EXPRESS

Texturing metal surface with MHz ultra-short laser pulses

FOTIS FRAGGELAKIS,[1,2] GIROLAMO MINCUZZI,[1,*] JOHN LOPEZ,[1,2] INKA MANEK-HÖNNINGER[2] AND RAINER KLING[1]

[1]*ALPhANOV, Technological Centre for Optics and Lasers, Optic Institute of Aquitaine, Rue F. Mitterrand 33400 Talence, France*
[2]*CELIA University of Bordeaux-CNRS-CEA UMR5107, 33405 Talence, France*
[*]*Girolamo.MINCUZZI@alphanov.com*

Abstract: We show, for the first time to our knowledge, the role the heat accumulation plays on the evolution of ultra-short pulse laser-induced surface structures morphology when varying fluence, the number of scans and the repetition rate from 100 kHz up to 2 MHz. We demonstrate how to tailor the size of micro-spikes from nearly ten microns to several tens of microns by a systematic variation of both fluence and overlap. We believe our results will contribute to an in deep understanding of the mechanisms underlying laser surface structuration at high repetition rates.

OCIS codes: (140.3390) Laser materials processing; (220.4000) Microstructure fabrication; (320.2250) Femtosecond phenomena; (140.6810) Thermal effects.

References and links

1. D. H. Kam, S. Bhattacharya, and J. Mazumder, "Control of the wetting properties of an AISI 316L stainless steel surface by femtosecond laser-induced surface modification," J. Micromech. Microeng. **22**(10), 105019 (2012).
2. M. Barberoglou, V. Zorba, E. Stratakis, E. Spanakis, P. Tzanetakis, S. H. Anastasiadis, and C. Fotakis, "Bio-inspired water repellent surfaces produced by ultrafast laser structuring of silicon," Appl. Surf. Sci. **255**(10), 5425–5429 (2009).
3. L. Gemini, M. Faucon, L. Romoli, R. Kling, R. F. Mitterrand, and I. Industriale, "High throughput laser texturing of super-hydrophobic surfaces on steel," Proc. SPIE **10092**, 1–6 (2017).
4. A. Y. Vorobyev and C. Guo, "Colorizing metals with femtosecond laser pulses," Appl. Phys. Lett. **92**(4), 1–4 (2008).
5. J.-M. Guay, A. C. Lesina, J. Baxter, M. Charron, G. Côté, L. Ramunno, P. Berini, and A. Weck, "Enhanced plasmonic coloring of silver and formation of large laser-induced periodic surface structures using multi-burst picosecond pulses," arXiv Prepr. 1609.04847, 1–8 (2016).
6. J. Bonse, R. Koter, M. Hartelt, D. Spaltmann, S. Pentzien, S. Hohm, A. Rosenfeld, and J. Kruger, "Femtosecond laser-induced periodic surface structures on steel and titanium alloy for tribological applications," Appl. Phys., A Mater. Sci. Process. **117**(1), 103–110 (2014).
7. E. Skoulas, A. Manousaki, C. Fotakis, and E. Stratakis, "Biomimetic surface structuring using cylindrical vector femtosecond laser beams," Sci. Rep. **7**, 45114 (2017).
8. S. Höhm, A. Rosenfeld, J. Krüger, and J. Bonse, "Femtosecond laser-induced periodic surface structures on silica," J. Appl. Phys. **112**(1), 014901 (2012).
9. M. Faucon, A. Laffitte, J. Lopez, and R. Kling, "Surface blackening by laser texturing with high repetition rate femtosecond laser up to 1MHz," Proc. SPIE **8972**, 89721M (2014).
10. S. K. Das, D. Dufft, A. Rosenfeld, J. Bonse, M. Bock, and R. Grunwald, "Femtosecond-laser-induced quasiperiodic nanostructures on TiO 2 surfaces," J. Appl. Phys. **105**, 084912 (2013).
11. S. K. Sundaram and E. Mazur, "Inducing and probing non-thermal transitions in semiconductors using femtosecond laser pulses," Nat. Mater. **1**(4), 217–224 (2002).
12. J. E. Sipe, J. F. Young, J. S. Preston, and H. M. Van Driel, "Laser-induced periodic surface structure. I. Theory," Phys. Rev. B **27**(2), 1141–1154 (1983).
13. J. Bonse, A. Rosenfeld, and J. Kruger, "On the role of surface plasmon polaritons in the formation of laser-induced periodic surface structures upon irradiation of silicon by femtosecond-laser pulses," J. Appl. Phys. **106**(10), 104910 (2009).
14. G. D. Tsibidis, M. Barberoglou, P. A. Loukakos, E. Stratakis, and C. Fotakis, "Dynamics of ripple formation on silicon surfaces by ultrashort laser pulses in subablation conditions," Phys. Rev. B **86**(11), 1–14 (2012).
15. G. D. Tsibidis, C. Fotakis, and E. Stratakis, "From ripples to spikes: A hydrodynamical mechanism to interpret femtosecond laser-induced self-assembled structures," Phys. Rev. B **92**(4), 041405 (2015).

#295932 https://doi.org/10.1364/OE.25.018131
Journal © 2017 Received 30 May 2017; revised 12 Jul 2017; accepted 13 Jul 2017; published 19 Jul 2017

Optics EXPRESS

16. G. Mincuzzi, L. Gemini, M. Faucon, and R. Kling, "Extending ultra-short pulse laser texturing over large area," Appl. Surf. Sci. **386**, 65–71 (2016).
17. E. J. Y. Ling, J. Saïd, N. Brodusch, R. Gauvin, P. Servio, and A. M. Kietzig, "Investigating and understanding the effects of multiple femtosecond laser scans on the surface topography of stainless steel 304 and titanium," Appl. Surf. Sci. **353**, 512–521 (2015).
18. D. H. Kam, J. Mazumder, and J. Kim, "Conical microspike morphology formation and control on various metal surfaces using femtosecond laser pulse," J. Laser Appl. **28**(4), 042001 (2016).
19. F. Bauer, A. Michalowski, T. Kiedrowski, and S. Nolte, "Heat accumulation in ultra-short pulsed scanning laser ablation of metals," Opt. Express **23**(2), 1035–1043 (2015).
20. C. Hönninger and J. Akhil, "Femtosecond Lasers over 100 Watts industrial applications," Laser Tech. J. **13**(2), 56–59 (2016).
21. W. L. Barnes, A. Dereux, and T. W. Ebbesen, "Surface plasmon subwavelength optics," Nature **424**(6950), 824–830 (2003).
22. N. M. B. Perney, J. J. Baumberg, A. Tang, M. C. Netti, M. D. B. Charlton, and M. E. Zoorob, "Tuning localized plasmon cavities for optimized surface-enhanced Raman scattering," Phys. Rev. B **7**, 1–5 (2007).
23. C. Wu and L. V. Zhigilei, "Microscopic mechanisms of laser spallation and ablation of metal targets from large-scale molecular dynamics simulations," Appl. Phys., A Mater. Sci. Process. **114**(1), 11–32 (2014).
24. R. Fang, A. Vorobyev, and C. Guo, "Direct visualization of the complete evolution of femtosecond laser-induced surface structural dynamics of metals," Light Sci. Appl. **6**(3), e16256 (2016).
25. F. Di Niso, C. Gaudiuso, T. Sibillano, F. Paolo, A. Ancona, and P. M. Lugarà, "Role of heat accumulation on the incubation effect in multi-shot laser ablation of stainless steel at high repetition rates," Opt. Express **22**, 2230–2236 (2014).
26. P. R. Gadkari, A. P. Warren, R. M. Todi, R. V. Petrova, and K. R. Coffey, "Comparison of the agglomeration behavior of thin metallic films on Si O 2 Comparison of the agglomeration behavior of thin metallic films on SiO 2," J. Vac. Sci. Technol. A **23**, 1152 (2014).
27. B. F. Donovan, J. A. Tomko, A. Giri, D. H. Olson, J. L. Braun, J. T. Gaskins, P. E. Hopkins, J. T. Gaskins, and P. E. Hopkins, "Localized thin film damage sourced and monitored via pump-probe modulated thermoreflectance," Rev. Sci. Instrum. **88**(5), 054903 (2017).
28. B. K. Nayak and M. C. Gupta, "Self-organized micro/nano structures in metal surfaces by ultrafast laser irradiation," Opt. Lasers Eng. **48**(10), 940–949 (2010).
29. F. Fraggelakis, G. Mincuzzi, J. Lopez, I. Manek-hönninger, and R. Kling, "Ultrashort pulse laser-induced texturing of stainless steel at 1 MHz and high average power : impact of process parameters," Proc. SPIE **10092**, 1–7 (2017).

1. Introduction

Material surface texturing by ultra-short pulse (USP) lasers is an attractive technology since it enables the tailoring of some highly interesting material properties. By inducing periodical (ripples) and quasi periodical surface structures (spikes), also referred as LIPSS (laser induced periodic surface structures) the material surface wettability behavior [1–3], optical aspects [2,4,5] and tribological properties [6] could change radically without the need of coatings. In fact, irradiating the surface of several materials [7–10] with USP lasers can lead to the formation of LIPSS, subsequently modifying the surface interaction properties. Multiple phenomena [11] have been considered to elaborate a complete model describing the LIPSS formation mechanism. We mention for instance photon- surface plasmon coupling [12,13] inducing periodical thermal gradients and subsequently, micro-fluidic reallocation of material, as a possible explanation of ripple formation [14]. Whereas, micro grooves and conical micro-spikes formation could be ascribed to material movement due to Marangoni flow, driven by a local thermal gradient [15]. In all these cases the time interval between two successive laser pulses is considered long enough to permit effective heat dissipation and phenomena which are related with the inter-pulses heat accumulation are not taken into account.

However, the exploitation of LIPSS into an industrial environment for commercial purposes requires implementing a reliable and effective production system whilst increasing the process throughput. This could be tackled utilizing very fast laser beam positioning systems delivering the beam with scanning speeds in the range of several tens of m/s [16] together with high power (tens of Watts), high repetition rate (MHz range) [17,18], industrial, ultra-short pulse laser systems. Nevertheless, surface processing at repetition rates within the MHz range, could induce inter-pulses heat accumulation, compromising the surface

Optics EXPRESS

morphology. During the irradiation with repetition rate values close to 1 MHz a metallic surface is expected to reach a saturation temperature of several hundreds of degrees [19]. Key process parameters such as the overlap, the fluence and the repetition rate are expected to impact this temperature.

In this work, we show for the first time to our knowledge a comparative study on stainless steel highlighting the impact of the fluence, the overlap and the number of successive scans on the surface morphology when passing from 100 kHz to 1 MHz and even up to 2 MHz. Moreover, in the case of high repetition rates (1 and 2 MHz) we show that by systematic variation of process key parameters, it is possible to tune the size of the micro-spikes while at the same time avoiding detrimental effects related to heat accumulation.

We believe that our results will contribute to a deeper understanding of the physical phenomena underlying the material surface texturing by MHz, USP lasers. Moreover, by showing a reliable way to exploit the full capabilities of up to date USP industrial laser sources [20] this study can open the way to export laser surface texturing into an industrial environment.

2. Experimental setup and process parameters

A commercial ultrafast fiber laser system (Tangerine, Amplitude Systèmes) emitting in the near infrared (λ = 1030 nm) with a maximum output power of 20 W and delivering ultra-short pulses of 350 fs was utilized for the texturing experiments. The delivered laser beam was linearly polarized and Gaussian with an M^2 = 1.1. We expanded the beam by a factor of 2 and focalized it with a 100-mm f-theta lens. The spot diameter, measured via a beam profiler (Win CAM), was $2\omega_0$ = 35 µm. With this setup we structured the surface of 316 L stainless steel samples of 0.5 mm thickness by scanning over the sample surface using a Galvo scanner (SCANLAB model IntelliSCAN 14 and hurrySCAN II 14).

The process parameters considered are the repetition rate (f), the fluence (Φ), the number of scans (N) and the pulses per spot (pps). The latter is defined as the average number of pulses irradiated in a dimentionless spot of the surface in a single scan calculated as pps = $(2\omega_0 \cdot f) / u$ where u is the scanning speed. Φ is defined as $E/(\pi \cdot \omega_0^2)$, where E is the energy of the pulse. The pps_{tot}, defined as pps · N, is a variable used to describe the total amount of pulses irradiated on the surface. The lateral overlap is not taken into account. Finally, the dose, which represents the total energy irradiated per unit surface, defined as $D = pps_{tot} \cdot \Phi$ could give both a quantitative as well as a more perceptible way to describe the amount of energy irradiated on the surface.

In our study we considered three different repetition rate values: 100 kHz, 1 MHz and 2 MHz. The fluence was varied between Φ = 0.04 J/cm^2 and Φ = 0.40 J/cm^2 by increasing the laser pulse energy from 0.3 µJ to 9 µJ. The overlap was chosen between 15 pps and 200 pps, and the number of successive scans N was varied between N = 1 and N = 500. The experimental parameters are summarized in Table 1.

Table 1. Summary of the experimental values used

Parameter	Minimum	Maximum
Repetition rate (f)	100 kHz	2 MHz
Fluence (Φ)	0.04 J/cm^2	0.40 J/cm^2
Pulse energy (E)	0.3 µJ	9 µJ
Number of scans (N)	1	500
Pulses per spot (pps)	15 pps	200 pps

The surface morphology analyses were carried out utilizing two scanning electronic microscopes (SEM), a CSEM-FEG INSPECT 50 and a FEI Phenom. By using a commercial software (Gwyddion) we analyzed the SEM images by measuring the surface area of the obtained structures. The equivalent spike size diameter δ presented in this work corresponds to the diameter of the circumference having the same surface than the spike surface. The

Optics EXPRESS

average δ values, in most cases, occur by measuring several hundreds of features in an SEM image.

For each set of process parameters, a 1 mm x 3 mm surface was raster scanned utilizing a hatch value of 10 μm. Finally, the material was cleaned in acetone ultrasonic bath in order to remove the ablation dust produced during the laser irradiation.

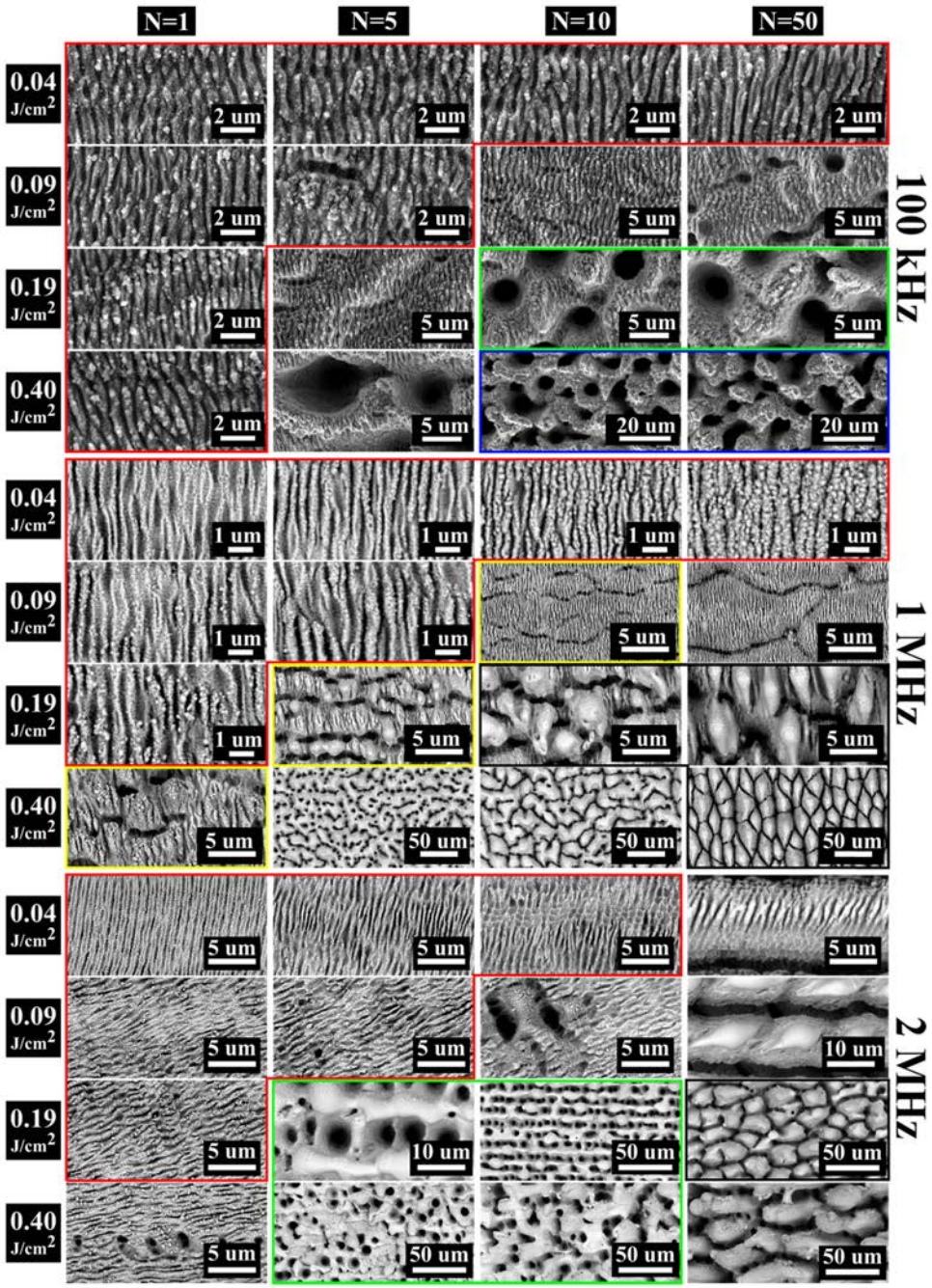

Fig. 1. SEM images of stainless steel surface obtained at different repetition rates as indicated. N indicates the number of scans in each column. The fluence Φ increases from top to bottom

Optics EXPRESS

and is the same in each row. The overlap was fixed to 70 pps. Different types of nanostructures are indicated with different colour frames.

3. Results and discussion

3.1 Evolution of surface morphology for 100 kHz, 1 MHz and 2 MHz

In this part, we present the results obtained by processing the samples with a fixed overlap (pps = 70) and by varying both the number of scans N (between N = 1 and N = 50) and the fluence Φ (between Φ = 0.04 J/cm^2 and Φ = 0.40 J/cm^2). The same combination of N and Φ was utilised for 3 repetition rates, f = 100 kHz, f = 1 MHz and f = 2 MHz. In Fig. 1 are shown the SEM surface structure morphologies we obtained.

For all the three f values, areas including similar structures can be distinguished by a different colour frame. Ripples, periodical formations, with a period close to the laser wavelength, occur for low dose values with an orientation perpendicular to the laser polarization and are identified by a red frame. Diverse types of grooves, which are formed parallel to the laser polarization with a period significantly larger than the laser wavelength are indicated by a yellow frame. Coral like structures are marked by a blue frame. Spikes, the conical formations with diameters in the range of tens of microns, formed for higher doses are indicated by a black frame and finally holes by a green frame.

The fact, that for higher doses, the same N and Φ values lead to different surface morphologies for different f values indicates the role of heat accumulation. For instance the couple Φ = 0.09 J/cm^2 and N = 50 enables the formation of ripples at f = 100 kHz (Fig. 1), micro-grooves superposed to ripples at f = 1 MHz (Fig. 1) and, finally, spikes at f = 2 MHz (Fig. 1). The combination Φ = 0.19 J/cm^2 and N = 10 enables the formation of a hole's net at 100 kHz, inhomogeneous spikes at 1 MHz and an inhomogeneous distribution of melted and re-casted material along the scanning axis at 2 MHz.

Summarizing, for values beyond ripple formation, the evolution of the material surface and its final surface morphology shows two distinctive behaviours at f = 100 kHz and when f is in the range of MHz.

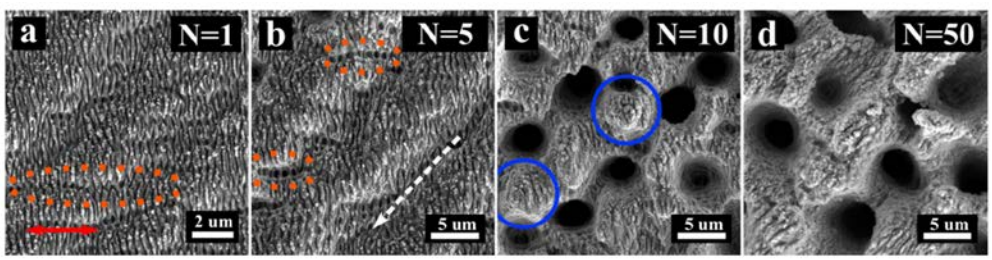

Fig. 2. SEM images showing the surface evolution at 100 kHz obtained with Φ = 0.19 J/cm2 and pps = 70. N indicates the number of scans. The red arrow shows the polarization direction, and the white dotted arrow indicates the scanning axis.

Figure 2 shows in detail how the material surface evolves for pps = 70, f = 100 kHz and Φ = 0.19 J/cm^2, when increasing the number of scans from N = 1 to N = 50 (Fig. 2(a)-2(d)). Starting from N = 1 (Fig. 2(a)), ripples are formed perpendicularly to the polarization direction (see red arrow). At the same time, shallow undulations arise parallel to the laser polarization. Their orientation and period are similar to micro grooves observed in solids [9,15]. Between the undulations, craters are generated (see orange ellipse) with an increasing number of scans (N = 5 Fig. 2(b)). We believe that both are resulting from lateral displacement of material. For N = 5 (Fig. 2(b)) the scanning hatch (see white arrows) impacts the surface with the formation of relatively wide and shallow, parallel, trenches spaced of 10 μm.

Optics EXPRESS

By increasing N, craters are transformed into holes of nearly 5 μm diameter (Fig. 2(c) and (d)). Very likely, this transformation can be attributed to an enhancement of light absorption around the crater: in particular, phenomena related to plasmonic resonances [21] and the local enhancement of the incident field [22], lead to locally increased ablation.

For N = 50 (Fig. 2 (d)) the predominant surface morphology becomes a net of 5 μm diameter micro-holes aligned along the laser scanning direction and regularly spaced of nearly 10 μm combined with a coral-like roughness. Spare spikes (see blue circle) are also formed but, in the range of the applied process parameters, micro-holes constitute the predominant morphology on the surface. In Fig. 1 we observe that the micro-hole diameter depends not only on the number of scans N, but, for a fixed N value, also on the fluence Φ and, the higher the fluence the larger the diameter. For instance, in the case of N = 50, the μ-hole diameter passes from nearly 1 μm ($\Phi = 0.09$ J/cm^2) to more than 5 μm ($\Phi = 0.40$ J/cm^2). Interestingly, once the μ-holes are formed, their number doesn't change remarkably with the variation of the process parameters. Moreover, the increase of the micro-hole diameter with Φ and N jointly with coral-like roughness ascertains, to a large extend, the prevailing of ultrafast ablation phenomena on thermofluidic effects in determining material removing and local material reallocation.

During the irradiation with repetition rates in the range of MHz, thermal effects are expected to arise. Residual heat remaining after the irradiation on the surface of the material [23] is dissipated into the bulk within the time frame of a millisecond [11,24]. In case of high repetition rates, the delay between the pulses becomes comparable with the time required for heat dissipation from the surface to the bulk. Under specific conditions, such as high overlap or fluence, residual heat builds up pulse after pulse. It has been demonstrated [19] that under high repetition rate irradiation (800 kHz, pulse duration of 10 ps) of stainless steel, heat is accumulated within a single scan preventing the temperature of the surface to decrease below a saturation temperature T_b. Depending on the process parameters, T_b could be in the range of several hundreds of degrees influencing the nanostructure formation. Each successive pulse further increases the surface temperature. For specific values of Φ and pps, the transient temperature could reach the melting point of the material. This phenomenon, being referred to as heat accumulation, observed in bulk materials [25], and in thin films [26,27], is as we believe the interpretation of the significantly different nanostructures shown in Fig. 2 and Fig. 3.

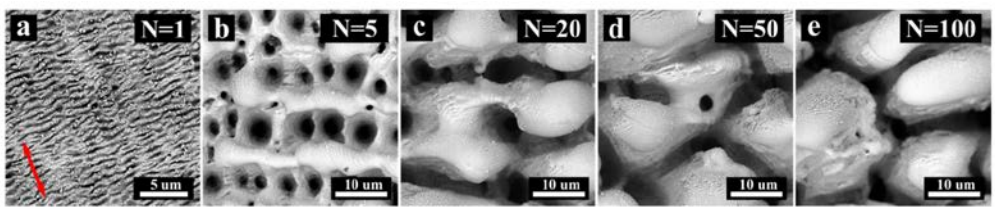

Fig. 3. SEM images showing the surface evolution at 2 MHz obtained with $\Phi = 0.19$ J/cm^2 and pps = 70. N indicates the number of scans. The red arrow shows the polarization direction.

Figure 3 illustrates the structures obtained for f = 2 MHz, $\Phi = 0.19$ J/cm^2 and pps = 70 while increasing N. For N = 5 (Fig. 3(b)), micro-holes of 5-10 μm diameter are already formed and distributed along the laser scanning lines. Compared with f = 100 kHz (Fig. 2), holes are formed for smaller number of scans when f = 2 MHz. Moreover, melted and re-casted material characterized by a smooth and bumpy external surface is clearly visible between two scanning lines spaced of nearly 10 μm. Increasing the number of scans to N = 20 (Fig. 3(c)) further movement of material tend to fill the holes and coalesce in larger aggregates consisting of bumpy protrusions. Finally, for N = 100 (Fig. 3(e)), the surface morphology mostly consists of a uniform distribution of bumpy spikes (referred as spikes). The equivalent average spike diameter δ was measured to be $\delta = 22 \pm 3$ μm. Interestingly,

Optics EXPRESS

once the spikes are formed δ is barely affected by increasing the number of scans, even for N >> 50 (δ = 22 ± 4 μm for N = 200). On the contrary, δ changes with the repetition rate f. Indeed, for Φ = 0.19 J/cm^2, N = 100 pps = 70 and f = 1 MHz we obtained δ = 14 ± 3 μm. This observation is consistent with the idea that the spike formation is driven by hydrodynamical flow resulting from temperature gradients [15]. Higher repetition rate is expected to lead to higher T_b and thus to a deeper penetration of the heat during the irradiation. As a consequence we expect the volume of the material subjected to Maragony driven flow to be more extended as f increases, subsequently leading to the formation of larger features.

3.2 The role of fluence on spike morphology

An extremely interesting aspect of the results reported in the previous paragraph lies in the correlation between the quantity of heat deposited into the material during the laser pass, and both the size and the morphology of the bumps. It can be argued that a fine control of the process parameters, such as fluence could be the key element to gauge the quantity of heat deposited. A dependence between fluence and spike size has been previously reported for low repetition rates in several metals [28]. Moreover, this behavior seems to be independent from the irradiation wavelength [29]. In the following part, we show the impact of the fluence on the induced structures for f = 1 MHz. In our experiment, we deliver the same number of pulses (pps_{tot} = 3500), using the same strategy in all cases (pps = 70 N = 50) and we varied the fluence between Φ = 0.11 J/cm^2 and Φ = 0.54 J/cm^2. Results are illustrated in Fig. 4.

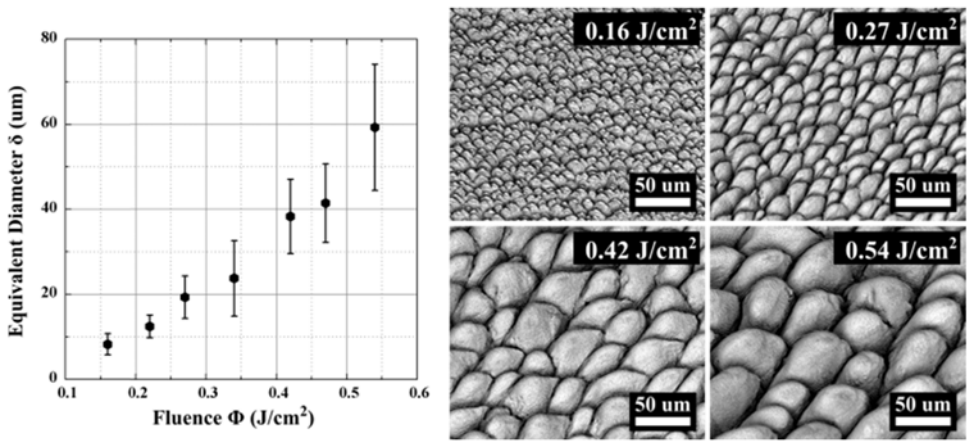

Fig. 4. SEM images (right) and graph (left) illustrating the continuing change of the equivalent diameter δ with increasing fluence. The SEM images correspond to the data shown on the graph and where obtained at a 45° tilt. The fluence values are inserted in the corresponding SEM images.

The graph (left) in Fig. 4 shows the δ values versus the fluence Φ. For relatively low fluence values (0 < Φ < 0.16 J/cm^2) no spikes are formed. In these experimental conditions, a uniform distribution of spikes comes out only beyond a threshold value of ≈0.16 J/cm^2 having an equivalent diameter δ = 8 ± 2 μm. Within the experimental fluence range (0.16 J/cm^2 < Φ <0.54 J/cm^2), δ increases monotonically from δ = 8 ± 2 μm to δ = 59 ± 15 μm. We therefore observe that it is possible to control the resulting spike size over a relatively wide range by varying the fluence. Interestingly, within the used fluence values unwanted thermal effect of the high repetition rate are avoided enabling the formation of uniform and well defined, bumpy surface structures.

Optics EXPRESS

3.3 The role of overlap on spike morphology

Recently, it has been shown [29] for 1 MHz that when keeping the same dose values, e.g. deliver the same number of pulses having the same fluence, is it possible to modify the spike morphology by varying the number of pulses per spot (pps). Furthermore, a correlation between overlap and T_b has been established in reference [19].

In the following sets of experiments we investigate the role of the overlap in spike formation for high repetition rates. The evolution of spike diameter versus the pps_{tot} is shown in Fig. 5, which illustrates the results for f = 1 MHz (left) and f = 2 MHz (right), respectively. For both f values two different pps values were considered i.e. pps = 70 and pps = 300 for 1 MHz and pps = 30 and pps = 70 for 2 MHz. Finally, a fixed fluence value (Φ = 0.19 J/cm^2) means that the same pps_{tot} corresponds to the same overall energy dose.

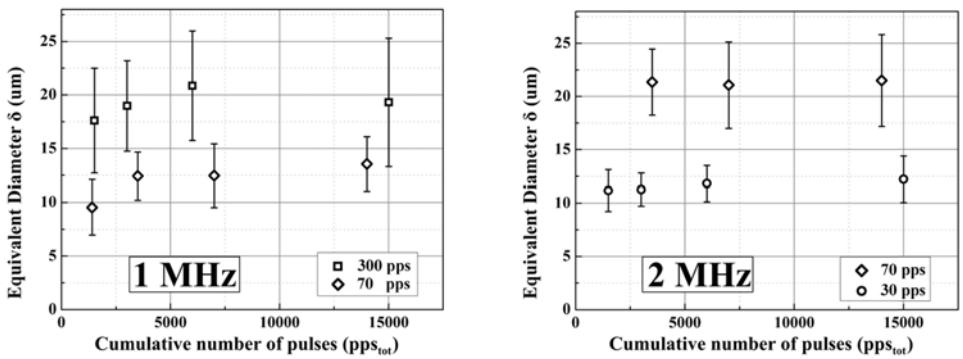

Fig. 5. Evolution of average equivalent spike diameter (δ) under successive scan irradiation for different overlaps and repetition rates. On the left side, the results obtained with f = 1 MHz, and on the right side those obtained for f = 2 MHz are shown. Different shapes indicate different overlaps. The fluence was constant in all cases (Φ = 0.19 J/cm^2).

Within our experimental conditions, spikes are formed starting from a threshold value of nearly pps_{tot} = 1400 independently of the overlap and the repetition rate. It can be clearly observed that δ increases, when the overlap (pps) increases. At 1 MHz, the initial diameter corresponding to similar doses is δ = 9.5 ± 2.5 μm for pps = 70 (pps_{tot} = 1400) and δ = 13.5 ± 2.5 μm for pps = 300 (pps_{tot} = 1500). In this case, we can extract an increment of roughly Δδ/Δpps = 0.0174 μm/pps. Variations in the value of overlap for 2 MHz seem to have more significant impact. For similar doses, the diameter is δ = 11 ± 2 μm for pps = 30 (pps_{tot} = 3000) and δ = 21 ± 3 μm for pps = 70 (pps_{tot} = 3500), respectively, showing an increment of Δδ/Δpps = 0.25 μm/pps. Finally, a dose value of pps_{tot} = 3500 delivered with the same strategy (N = 50, pps = 70) will lead to structures with δ = 12.5 ± 2 μm for f = 1 MHz and δ = 21 ± 3 μm for f = 2 MHz, highlighting the brunt of repetition rate in the thermofluidic mechanism that leads to spike formation.

Moreover, a specific trend in spike evolution is observed as the pps_{tot} increases. Starting from 1 MHz we observe for 1400 ≤ pps_{tot} < 5000, δ clearly increases and tends to be stable for pps_{tot}> 5000 reaching a saturation value δ_s which is δ_s = 13.5 ± 2.5 μm for pps = 70 and δ_s = 19.5 μm ± 6 μm for pps = 300, respectively. On the contrary for 2 MHz the spike size doesn't change after they emerge and the saturation value varies between δ_s = 11 μm ± 2 μm for pps = 30 and δ_s = 21 μm ± 3 μm for pps = 70, respectively. Saturation in the growth of spikes could be interpreted by the fact that the delay between two successive scans is much longer than the time required for the diffusion of the heat accumulated during one laser scan.

Therefore, it can be concluded that for fixed fluence and dose values the impact of the pulse overlap and repetition rate on the spike morphologies is confirmed at 1MHz and 2 MHz. Furthermore, after reaching a certain pps_{tot} threshold value it is even possible to use the overlap as an effective knob to finely tune the spike size.

Optics EXPRESS

4. Conclusions

We carried out a comprehensive study on the influence of process parameters, such as fluence, repetition rate, overlap and pulse per spot, on the laser induced structures at high repetition rates (up to 2 MHz). The impact of the heat accumulation on the structures morphology when the repetition rate is in the MHz regime has been reported. Interestingly, different morphologies are obtained for different repetition rates values also when the rest of process parameters (fluence, overlap and number of scans) are identical. We have shown a correlation between both pulse per spot and fluence values and the spikes size providing a useful tool to tune the spikes morphology. By comparing the results obtained at 100 kHz and 2 MHz we attempt an interpretation of the possible mechanisms that drives the evolution of the surface morphology. Our interpretation is consistent with the idea that spike formation is ascribed to thermo-fluidic phenomena driven by temperature gradients. Finally, our study will contribute to a deeper understanding of the spike formation process providing at the same time a useful tool for controlling their size.

Funding

Horizon 2020 Framework Programme (H2020) under the Marie Skłodowska-Curie grant agreement (No 675063).

Acknowledgments

The authors acknowledge “Laboratorio de Microscopías Avanzadas” in Zaragoza (Spain) and Mr. C. C. Ayllón for his very useful contribution to SEM characterization.